EPJ manuscript No.
(will be inserted by the editor)

Nonequilibrium photo dynamics of low-dimensional strongly correlated electron systems

Takami Tohyama[a]

Yukawa Institute for Theoretical Physics, Kyoto University, Kyoto 606-8502, JAPAN

Abstract. One of the outstanding contemporary challenges in condensed matter physics is to understand the dynamics of interacting quantum systems exposed to an external perturbation. We theoretically examine nonequilibrium photo dynamics and its interplay of charge, spin, and lattice degrees of freedom on a Hubbard-Holstein chain in one dimension and a t-J-Holstein square lattice in two dimensions. In the chain, performing dynamical density-matrix renormalization group calculations, we find that many phonons generated dynamically after photo irradiation in Mott insulators cause initial relaxation process. On the other hand, in the square lattice with model parameters as relevant for cuprates, a Lanczos-type exact diagonalization calculation shows that the majority of absorbed energy flows into spin subsystem rather than phonon subsystem.

1 Introduction

Ultrafast transient optics is an approach exploring new functionalities of materials and observing properties hidden in equilibrium conditions. Photons injected to the materials change their states from the ground state to nonequilibrium-steady states via initial relaxation processes within sub-picosecond scale. In strongly correlated electron systems, interdependence among spin, charge, orbital, and lattice degrees of freedom is crucial for not only the ground state but also photo-excited states. Low-dimensional transition metal oxides and organic materials with strong electron correlation are now targets for the investigation of photo-induced nonequilibrium states [1].

In this review, we address a fundamental, yet unresolved question concerning the interplay between strong correlation and electron-phonon (EP) interaction in a driven quantum system far from equilibrium. The electric field directly couples to the charge degrees of freedom. Thus, the EP interaction contributes to the initial relaxation of the excited state. In strongly correlated systems, there exists the spin degree of freedom, which is also possible to make a contribution to the relaxation. In one dimension (1D), the decoupling of spin and charge degrees of freedom, called spin-charge separation, observed in low-energy excitations may give rise to less relaxation processes to the subsystem of spin. On the other hand, in two dimensions (2D), charge can be coupled

[a] e-mail: tohyama@yukawa.kyoto-u.ac.jp

to spin because the charge motion creates the rearrangement of spin bonds [2]. It is, therefore, important to clarify the dependence of the initial relaxation process on dimensionality, which may resolve the question on the interplay between strong correlation and EP interaction.

In this paper, the relaxation process of 1D Mott insulators coupled with phonons is discussed in Sec. 2. We introduce the Einstein phonons and Holstein-type EP coupling. In order to see the effect of phonons on optical response, we examine optical conductivity in the Hubbard-Holstein model by the dynamical version of the density-matrix renormalization group (DMRG) [3]. Furthermore, the time dependent vector potential of laser pulse is incorporated into the 1D Hubbard-Holstein model. Examining initial relaxation after irradiation by time-dependent DMRG, we find that spin-charge coupling existing for strong excitation is suppressed with introducing small magnitude of EP coupling. At the same time, many phonons are excited dynamically in the system. This dynamical generation of phonons characterizes phonon relaxation in Mott insulators [4].

In Sec. 3, we examine single hole motion of the t-J-Holstein model as a representative example of 2D systems. It is known that the model can describe cuprate superconductors. By the comparison between the energy absorbed by the spin subsystem and the one absorbed by lattice vibrations, it is found that the spin subsystem absorbs the energy from the electric field more efficiently than the lattice for model parameters for cuprates [5].

These results lead to the conclusion that the initial relaxation process in Mott insulators coupled to phonons is governed by the phonon degree of freedom in 1D and by the spin degree of freedom in 2D. This may give information on the interpretation of ultrafast photo dynamics observed in 1D insulating cuprates [6] and organic materials [7–9] as well as 2D insulating cuprates [10].

2 One-dimensional Mott insulators coupled with Einstein phonon

The 1D Mott insulators, Sr_2CuO_3 and halogen-bridged Ni compounds, show photoinduced insulator-to-metal transition accompanied with its picosecond recovery to the insulating state [6,7]. The time scale of the recovery is three order of magnitude faster than that for semiconductors [11]. The 1D Mott insulators also exhibit gigantic third-order optical nonlinearity, and because of these two properties, they are promising future opto-electronics materials [12]. The complete description of optically excited Mott insulators and its nonequilibrium dynamic are thus desired.

The photocarriers of the 1D Mott insulators are called holon and doublon representing empty and doubly occupied sites, respectively. A holon and a doublon recombine by emitting energy to other elementary excitations. A problem is to clarify a pass way of energy flow due to the recombination. Possible candidates are of spin and phonon subspaces, since antiferromagnetic (AF) exchange energy and highest phonon frequencies are of the same order ($\sim$0.1 eV). Since high-energy states created by optical excitation may violate the separation of spin and charge degrees of freedom inherent in 1D electron systems [13], a pass way for energy flow through a spin channel can be expected. However, recent numerical studies have shown robustness of the spin-charge separation for nonequilibrium steady states [14,15]. It is thus necessary to make clear a coupling of spin and charge degrees of freedom under photoirradiation. As for phonon relaxation, pump-probe experiments have been done for various TTF-TCNQ salts with different magnitudes of EP coupling [8]. K- and Rb-TCNQ show spin-Peierls (SP) transition at T_c =395 K and 220 K, respectively, and their photocarriers are once localized as polarons at around 70 fs, and then recombine with a few ps. On the other hand, ET-F_2TCNQ does not show SP transition, and metallic

photocarriers decay within 200 fs. Therefore, a fundamental question to be answered is about what is driving force of ultrafast relaxation of the 1D Mott insulators when the charge carriers couple weakly with spin and lattice.

2.1 Hubbard-Holstein model

A coupling between an electron and breathing phonons in cuprates can be mapped onto Holstein- and Peierls-type EP interactions [16,17]. Since the Holstein interaction is stronger than the Peierls one, we consider the 1D Hubbard-Holstein model. In addition, a nearest-neighbor Coulomb repulsion that leads to excitonic effects is introduced. The resulting Hubbard-Holstein Hamiltonian is defined by

$$H = -t\sum_{i,\sigma}(c^{\dagger}_{i,\sigma}c_{i+1,\sigma} + \text{H.c.}) + U\sum_{i} n_{i,\uparrow}n_{i,\downarrow} + V\sum_{i}(n_i - 1)(n_{i+1} - 1) \\ +\omega_0\sum_{i} b^{\dagger}_i b_i - g\sum_{i}(b^{\dagger}_i + b_i)(n_i - 1), \tag{1}$$

where $c^{\dagger}_{i,\sigma}$ ($c_{i,\sigma}$) is the creation (annihilation) operator of an electron at site i with spin σ, and $b^{\dagger}_i$ (b_i) is the creation (annihilation) operator of a phonon at site i. This model includes electron hopping, t, on-site and nearest-neighbor Coulomb repulsions, U and V, respectively, phonon frequency, ω_0, and EP coupling, g. Keeping cuprates in mind, we take U larger than the band width $4t$.

2.2 Optical conductivity of Sr_2CuO_3

Let us examine the optical conductivity of the 1D Hubbard-Holstein model (1) at half-filling to understand basic nature of photoexcitation of the model. According to both experiment and effective spin model [19], phonon-assisted spin excitations with very small intensity are expected at the low-energy region well below the Mott gap.

By using dynamical current-current correlation function $\chi_j(\omega)$, the optical conductivity at zero temperature is given by $\chi_j(\omega)/\omega$. From the linear response theory, $\chi_j(\omega)$ reads

$$\chi_j(\omega) = \frac{1}{\pi N_{\rm s}}\text{Im}\,\langle 0|\, j^{\dagger}\frac{1}{\omega - H - \epsilon_0 - i\gamma}j\,|0\rangle\,, \tag{2}$$

where N_s is the number of electron sites, $j \equiv it\sum_{i,\sigma}(c^{\dagger}_{i+1,\sigma}c_{i,\sigma} - \text{H.c.})$ is the current operator, $|0\rangle$ is the ground state with eigenvalue ϵ_0, and γ is a infinitesimally small energy. Equation (2) for the Holstein-Hubbard model is calculated by using a dynamical DMRG method [18], where a multitarget procedure is employed. The multitarget states corresponding to the optical conductivity (2) are $|0\rangle$, $j\,|0\rangle$, and the correction vector $[\omega - H - \epsilon_0 - i\gamma]^{-1}\,j\,|0\rangle$.

For the calculation of the correction vector, a kernel polynomial expansion [20] is used [3]. This method uses a Gaussian broadening instead of the Lorentzian broadening expected from Eq. (2). The tail of the Lorentzian extends to a wide range of energy and the tail sometimes covers a small spectral weight. Actually, the Mott-gap excitations at high energy tend to hide the phonon-assisted spin excitations at low energy, since the weight of the former is more than thousand times larger than that of the latter as shown below. The Gaussian broadening can diminish such a undesirable tail [3].

A set of parameters of the Hubbard-Holstein model (1) that reproduces well both phonon-assisted spin excitation and Mott-gap excitation simultaneously in the optical

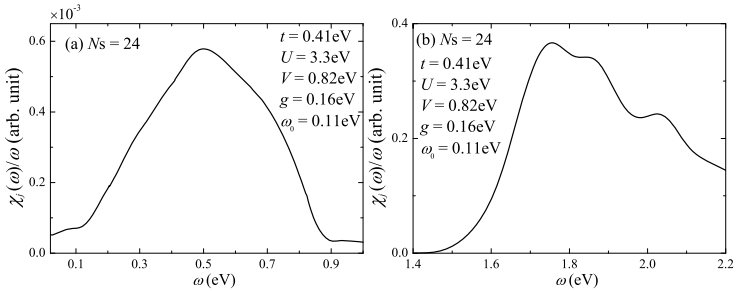

Fig. 1. Optical conductivity in a Hubbard-Holstein chain with 24 sites, taken from Ref. [3]. (a) Phonon-assisted spin excitation, and (b) Mott-gap excitation. The broadening factor $\sigma = 0.04$ eV. Parameter values are shown in the panels.

absorption of Sr_2CuO_3 has been determined in the following way. The phonon energy ω_0 is taken to be $\omega_0 = 0.11$ eV from experimental phonon peak at the bottom of phonon-assisted spin excitation [19], Since an excitonic peak seems to exist [21], a condition for V to generate the excitonic peak in 1D Mott insulator, $V/t = 2$ [22–24], is taken. Remaining parameters are t, U, and g. From a comparison of optical conductivity between experiment and dynamical DMRG calculation, a relation of $U/t \sim 8$ has been suggested [25,26]. For g, a diagrammatic Monte Carlo simulation reported a good description of angle-resolved photoemission spectra in 2D cuprates at half-filling when $g/t \sim 0.4$ [27]. Turning the ratios of U/t and g/t together with the value of t, a best parameter set that can describe both the Mott-gap and phonon-assisted spin excitations in different energy regions has been obtained [3]; $t = 0.41$ eV, $U = 3.3$ eV, $V = 0.82$ eV, $g = 0.16$ eV, and $\omega_0 = 0.11$ eV. The exchange interaction given by a $1/U$ expansion, $J = 4t^2/(U-V) = 0.273$ eV, is close to the experimentally estimated values, $J \sim 0.26$ eV [19,28].

Figure 1 shows optical conductivity at zero temperature for a 24-site chain under open boundary condition obtained by using the best parameter set [3]. The phonon-assisted spin excitations is shown in Fig. 1 (a). A phonon peak appears at *omega* ~ 0.08 eV. Above the phonon peak, a broad structure emerges as phonon-assisted spin excitations. The energy position of a broad peak, $\omega \sim 0.48$ eV, is consistent with an experimental value [19]. The peak comes from a Van Hove singularity of spinon excitation [19,29]. Figure 1 (b) shows the optical conductivity across the Mott gap. A peak appears at $\omega = 1.75$ eV. This energy is in agreement with the experimental data [30]. In addition, we can find a hump structure at $\omega = 1.86$ eV. It is natural to assign the hump structure to a one-phonon excitation on top of the $\omega = 1.75$ eV structure because of $\omega_0 = 0.11$ eV. Thus EP interaction contributes to the broadening of the main peak in the optical conductivity [31]. The intensity of the Mott-gap excitation is several hundred times larger than that of the phonon-assisted spin excitation, which is consistent with the experimental data [19]. Judging from the agreement of calculated spectral weights with experimental ones for both the Mott-gap excitation and phonon-assisted spin excitation, we conclude that the Hubbard-Holstein model with the suggested parameter set can describe very well the optical properties of Sr_2CuO_3. In the next subsection, we will examine nonequilibrium dynamics of the same model.

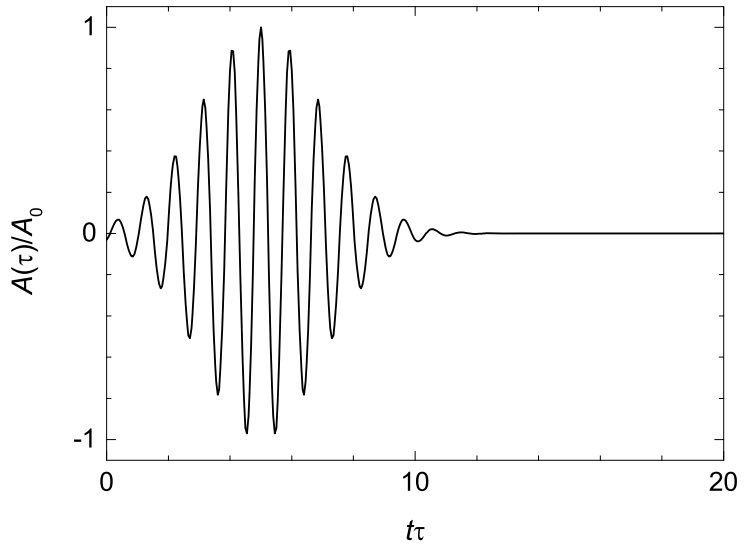

Fig. 2. Time-dependent vector potential $A(\tau)$ of pump light. $\tau_d = 2/t$, $\tau_0 = 5/t$, and $\omega_{\rm pump} = 6.75t$ in Eq. (3).

2.3 Relaxation Dynamics of Photocarriers

We introduce the time-dependent external electric field into the 1D extended Hubbard-Holstein model as the classical vector potential $A(\tau)$ of pump light. This is achieved by multiplying the Peierls phase $e^{iA(\tau)}$ to the hopping operators $c^\dagger_{i,\sigma}c_{i+1,\sigma}$, where $A(\tau)$ is defined by

$$A(\tau) = A_0 e^{-(\tau-\tau_0)^2/(2\tau_d^2)} \cos(\omega_{\rm pump}(\tau-\tau_0)). \tag{3}$$

Here τ_d is the duration time, τ_0 is the central position in time where the amplitude exhibits maximum, and $\omega_{\rm pump}$ is the frequency of pump laser. In Ref. [4], τ_d and τ_0 are fixed to be $\tau_d = 2/t$ and $\tau_0 = 5/t$, respectively, and $\omega_{\rm pump} = 6.75t$ whose value is tuned to the lowest-energy peak position of the optical conductivity. Figure 2 shows $A(\tau)$ obtained by using these values.

Photodoping rate due to pumping, δ, which is controlled by the amplitude of laser pulse A_0 in Eq. (3), is defined by

$$\delta = \lim_{\tau\to\infty} (E(\tau) - E_0)/(L\omega_{\rm pump}), \tag{4}$$

where L is the system size and $E(\tau) = \langle\tau| H |\tau\rangle$. $|\tau\rangle$ is the solution of the time-dependent Schrödinger equation, $i(\partial/\partial\tau)|\tau\rangle = H(\tau)|\tau\rangle$, and the solution is given by

$$|\tau\rangle = T\exp\left\{-i\int_0^\tau H(\tau')d\tau'\right\}|0\rangle \tag{5}$$

with T being the time ordering operator.

The time evolution of doublon number, $N_{\rm d}(\tau)$, phonon number, $N_{\rm ph}(\tau)$, and local spin correlation, $C_{\rm s}(\tau)$ are defined by

$$N_{\rm d}(\tau) = \sum_i \langle\tau| n_{i,\uparrow}n_{i,\downarrow} |\tau\rangle, \tag{6}$$

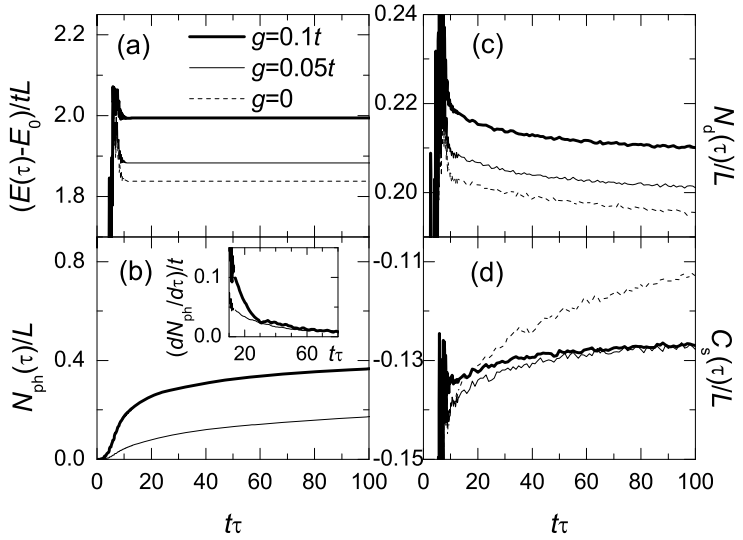

Fig. 3. Time evolution of various quantities in an extended Hubbard-Holstein chain with $L = 12$ taken from Ref. [4]. The bold solid, the fine solid, and the dashed lines represent the cases with $g = 0.1t$, $g = 0.05t$, and $g = 0$, respectively. (a) $E(\tau) - E_0$, (b) $N_{\rm ph}(\tau)$, (c) $N_{\rm d}(\tau)$, and (d) $C_{\rm s}(\tau)$. The inset of (b) represents the first derivative of $N_{\rm ph}(\tau)$. $A_0 = 2.0$. Pump-laser irradiation continues up to $\tau \sim 10/t$.

$$N_{\rm ph}(\tau) = \sum_i \langle \tau | \, b_i^\dagger b_i \, | \tau \rangle \,, \tag{7}$$

and

$$C_{\rm s}(\tau) = \sum_i \langle \tau | \, \mathbf{S}_i \cdot \mathbf{S}_{i+1} \, | \tau \rangle \,. \tag{8}$$

For numerical calculation of these time-dependent quantities, the DMRG technique is employed in Ref. [4], where a DMRG run for a given time τ is performed with repeating this for many τ. The detail of the calculation is described in Ref. [4]. In the calculation, a half-field $L = 12$ Hubbard-Holstein chain with open boundary condition is used. The parameters U, V, and ω_0 in (1) are taken to be $10t$, $2t$, and $0.1t$, respectively, which are almost the same as the values estimated in the previous subsection. The number of phonon is taken up to 6 states per phonon site.

In Fig. 3, we show time evolution of $E(\tau)$, $N_{\rm d}(\tau)$, and $C_{\rm s}(\tau)$ for $g = 0$, $g = 0.05t$, and $g = 0.1t$. The photodoping rate δ is set to be roughly 0.3 (see Eq. (4)) depending on g. At $g = 0$, i.e., without EP coupling, $E(\tau)$, $N_{\rm d}(\tau)$, and $C_{\rm s}(\tau)$ gradually increase during photoirradiation as expected. After the pumped pulse has been turned off ($\tau \geq 10/t = 2\tau_0$), $E(\tau)$ is hardly changed because of treating a closed system. We find that $N_{\rm d}(\tau)$ decreases as $C_{\rm s}(\tau)$ increases with time. The gradual increase of $C_{\rm s}(\tau)$ is not clearly observed in cases of weak excitation, i.e., small A_0 cases [13]. The decrease of $N_{\rm d}(\tau)$ and the increase of $C_{\rm s}(\tau)$ mean that holon and doublon created by pump pulse recombine with each other and the recombination is accompanied by an energy flow from the photocarriers to the spin degree of freedom. However, it should be noted that the slope of $C_{\rm s}(\tau)$ is very gradual. Furthermore, the change of $C_{\rm s}(\tau)$ from $t\tau = 10$ to 50 ($\sim$0.2) is smaller than the value of one spin flip ($\sim$1.0). Therefore, relaxation through the spin channel is not efficient in the extended Hubbard model,

even though the spin-charge coupling becomes evident as the pump power increases. This is qualitatively consistent with recent reports showing robustness of the spin-charge separation for nonequilibrium steady states [14,15].

For finite value of g in Fig. 3, the doublon number $N_{\rm d}(\tau)$ decreases after pumping ($t\tau > 10$), as is the case without EP coupling. Spin correlation is also reduced. However, the reduction of spin correlation is suppressed by increasing EP coupling, as is seen in Fig. 3(d). This implies the suppression of spin-charge coupling due to the presence of EP coupling.

The number of phonons increases after pumping as shown in Fig. 3(b). For $g = 0.1t$, $N_{\rm ph}(\tau)$ has two regions in the time domain after pumping ($t\tau > 10$): $N_{\rm ph}(\tau)$ increases rapidly and the slope changes at $t\tau \sim 30$ as is seen in the first derivative of $N_{\rm ph}(\tau)$ [the inset of Fig. 3(b)], followed by a gentle slope for $t\tau > 30$. This characteristic time of kink $\tau \sim 30/t$ roughly corresponds to the duration time of laser pump ($\sim 10/t$) plus the inverse of effective EP coupling, $(\lambda t)^{-1} = 20/t$. In a case with $g = 0.05t$, the inverse EP coupling is $(\lambda t)^{-1} = 80/t$, and the change in the slope is expected to occur at around $\tau \sim 90/t$. However, the kink structure is not clearly seen, since the coupling is too small. The rapid increase of phonon during $10/t < \tau < 30/t$ indicates an energy transfer from charge degree of freedom to phonon one in the initial stage of relaxation. In other words, initial relaxation is dominated by phonons.

In the following, let us examine the mechanism of phonon relaxation in light of the presence of the two time regions. As shown in Fig. 3(b), the expectation value of phonon number per site is less than one, but the size of local phonon Hilbert space taken in the calculations is huge. Then, we have two possibilities for the relaxation processes. The first one is that the recombination of a holon and a doublon is accelerated by the phonon emission, if these carriers were still mobile against the EP coupling. In this case, the relaxation has been almost finished at around $t\tau = 30$. On the other hand, if the phonon generation makes these carriers polaronic, the time scale $t\tau = 30$ represents the polaron formation, eventually leading to slow recombination dynamics in the later time region. In the present case with $g = 0.1t$, the former scenario is realized. We have tried preliminary calculation of a correlation function $\langle\tau|\, b_j^\dagger b_j n_{i,\uparrow} n_{i,\downarrow}\,|\tau\rangle$ in a 6-site chain, and have actually confirmed that the spatial distribution of phonons around photocarriers is uniform. When we take $g = 0.2t$, the distribution starts to concentrate on the photocarrier site. The detailed results will be shown elsewhere.

Let us also estimate the typical value of the time $t\tau = 30$. Our parameter set roughly corresponds to that for ET-F_2TCNQ, since g hardly affects the optical conductivity. The band width of the optical conductivity of our single-band model is $8t$, and experimentally the main band is located at around $0.5 \sim 2.1$ eV. Then, the electron hopping is estimated to be 0.2 eV. In this case, we obtain $\tau = 30/t \sim 100$ fs. This value is not contradictory to the value 200 fs for ET-F_2TCNQ [8].

3 Two-dimensional t-J model coupled with Holstein phonon

In this section, we consider nonequilibrium charge dynamics of a doped strongly correlated system coupled to phonons, where the energy gained by the motion of a charge carrier along the field is absorbed by quantum spin and phonon degrees of freedom which are all explicitly included in the model. We study a single charge carrier doped into a 2D plane within the t-J-Holstein model, which is a prototype model for the description of competing interactions in cuprate superconductors. We address a fundamental, yet unresolved question concerning the interplay between strong correlation and EP interaction in a driven quantum system far from equilibrium.

3.1 t-J-Holstein model and numerical method

We define the time-dependent t-J-Holstein Hamiltonian as

$$H_{tJ\mathrm{H}} = H_t(A) + H_J + H_{\mathrm{H}} \tag{9}$$

with

$$H_t(A) = -t \sum_{\langle i,j\rangle,\sigma} \left(\mathrm{e}^{iA(\tau)} \tilde{c}^{\dagger}_{i,\sigma} \tilde{c}_{j,\sigma} + \mathrm{H.}c. \right), \tag{10}$$

$$H_J = J \sum_{\langle i,j\rangle} \mathbf{S_i} \cdot \mathbf{S_j}, \tag{11}$$

$$\tag{12}$$

and

$$\begin{aligned} H_{\mathrm{H}} &= H_g + H_{\omega_0} \\ &= g \sum_i n_j (b^{\dagger}_i + b_i) + \omega_0 \sum_i b^{\dagger}_i b_i, \end{aligned} \tag{13}$$

where $\tilde{c}_{i,\sigma} = c_{i,\sigma}(1 - n_{i,-\sigma})$ is a projected electron operator, and $\langle i,j\rangle$ denotes a nearest-neighbour pair.

It is known that the total momentum of the single-hole ground state of the t-J model is at $\mathbf{k}_0 = (\pi/2, \pi/2)$ [2]. The ground state is calculated by exact diagonalization defined over a limited functional space [32–34]. To construct functions of the Hilbert space after N_h operations, we use the off-diagonal parts of Eq. (9) in the basis generator

$$\left\{ |\varphi^{N_h}_l\rangle \right\} = [H_t(A=0) + H_J + H_{\mathrm{H}}]^{N_h} |\varphi_0\rangle, \tag{14}$$

where $|\varphi_0\rangle = c_{\mathbf{k}_0}|\text{Néel}\rangle$ represents a translationally invariant state of a carrier in the Néel background.

We switch on the static uniform electric field F along the diagonal, i.e., the (1,1) direction, at time $\tau = 0$ and perform the time evolution by iterative Lanczos method [35]. Accordingly, we define the charge current $j(\tau)$ along the diagonal and set $A(\tau) = -F\tau/\sqrt{2}$ for positive $\hat{x}$ and $\hat{y}$ direction. We measure F in units of $[t/ea]$ with electric charge e and lattice spacing a, and set $e = a = 1$. The strength of the numerical method used is in construction of the Hilbert space that enables not only an accurate description of the ground state of the spin-lattice polaron, but it allows for enough extra spin and phonon excitations to absorb energy, emitted by the field driven carrier, until the system reaches the quasistationary state.

3.2 Relaxation dynamics of single hole

We focus mostly on weak and moderate values of EP coupling $\lambda = g^2/8t\omega_0$ and different regimes of ω_0, while keeping $J/t = 0.3$ constant.

It is interesting to perform the calculation of energy flow to the spin and phonon subsystem during applying electric field. The dynamics of a single carrier in dissipative medium enables investigation of the steady growth of energy due to carrier propagation in initially undistorted background at $T = 0$ [5]. The energy increase with time for spin and phonon degree of freedom is defined as

$$\Delta E_J(\tau) = \langle \tau | H_J | \tau \rangle - \langle 0 | H_J | 0 \rangle \tag{15}$$

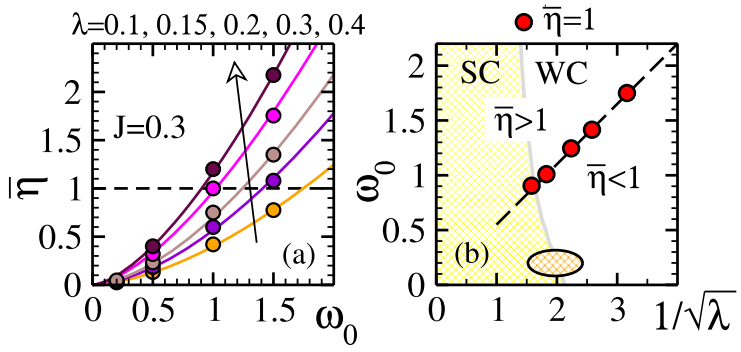

Fig. 4. (Color online) (a) $\bar{\eta}$ vs. ω_0 for different λ and $J/t = 0.3$. The arrow represents the direction from small to large λ. (b) Red dots denote values of $\omega_{0,\bar{\eta}=1}$ for which the condition $\bar{\eta} = 1$ is fulfilled, and dashed line represents a fit $\omega_{0,\bar{\eta}=1} = c/\sqrt{\lambda}$, with $c = 1.83$. Left and right side of the plot correspond to the strong coupling (SC) and weak coupling (WC) regime of EP coupling, respectively. Filled ellipse represents parameters as relevant for cuprates. Taken from Ref. [5].

and

$$\Delta E_{\omega_0}(\tau) = \langle \tau | \, H_{\omega_0} \, | \tau \rangle - \langle 0 | \, H_{\omega_0} \, | 0 \rangle \,, \tag{16}$$

respectively. Defining the energy flows to both subsystems as $\mathcal{P}_J(\tau) = d\Delta E_J(\tau)/dt$ and $\mathcal{P}_{\omega_0}(\tau) = d\Delta E_{\omega_0}(\tau)/dt$, we can obtain the distribution ratio $\eta(\tau) = \mathcal{P}_{\omega_0}(\tau)/\mathcal{P}_J(\tau)$. In the quasistationary state both $\Delta E_J(\tau)$ and $\Delta E_{\omega_0}(\tau)$ reveal a linear τ dependence [5], and therefore $\eta(\tau) = \bar{\eta}$, being τ independent. It has also been found that $\bar{\eta}$ remains fairly field F independent [5], altough the result is rather surprising since F strongly influences the energy flow into the system.

This result facilitates the investigation of the efficiency of the energy absorption through spin and phonon channel when the EP coupling and phonon frequencies are varied. With increasing ω_0, $\bar{\eta}$ increases at fixed λ as seen in Fig. 4(a). We are interested in the case $\bar{\eta} = 1$, i.e., when a propagating carrier deposits equal amount of the gained energy to the spin and the phonon subsystem alike. For this purpose, $\omega_{0,\bar{\eta}=1}$ that fulfills the equality condition $\bar{\eta} = 1$ is calculated and plottd as a function of λ in Fig. 4(b). Remarkably, a scaling $\omega_{0,\bar{\eta}=1} \sim 1/\sqrt{\lambda}$ is found. In the weak coupling regime the energy flow to phonons dominates over the flow to the spin subsystem only for large values of $\omega_0 > 1$. Recent angle-resolved photoemission [36,33] and optical experiments [37–39] on cuprates that were interpreted within the t-J-Holstein model, assigned the realistic λ to be in the interval $[0.2, 0.3]$ and $\omega_0 \sim 0.2$, as indicated by the filled ellipse in Fig. 4(b). In the parameter regime as relevant for cuprates, the majority of the absorbed energy via the charge carrier driven by the constant electric field flows in the spin subsystem. This is different from the case in 1D where the energy flow to the phonon subsystem is dominant as discussed in Sec. 2.3.

4 Summary

In this review, nonequilibrium photo dynamics and its interplay of charge, spin, and lattice degrees of freedom on a Hubbard-Holstein chain in one dimension and a t-J-Holstein square lattice in two dimensions have been investagated by numerical methods that are suitable for the models.

In the chain, a half-fielld Mott insulating state is the ground state. By using a parameter set that is suitable for an 1D cuprate Sr_2CuO_3, a dynamical DMRG calculation has clearly shown the presence of phonon-assisted spin excitations in the optical conductivity, which is consistent with experimetal observations. In order to clarify the physics of initial relatiation process of a photoexcited 1D Mott insulator, we have discussed the results obtained by time-dependent DMRG. The spin-charge coupling existing for strong excitation is suppressed with introducing small magnitude of EP coupling, and many phonons are excited dynamically in the system. This dynamical generation of phonons characterizes phonon relaxation in the 1D Mott insulator.

In the 2D square lattice, a single hole motion of the t-J-Holstein model under the constant electric field has been discussed. By the comparison between the energy absorbed by the spin subsystem and the one absorbed by lattice vibrations, it is found that the spin subsystem absorbs the energy from the electric field more efficiently than the lattice for model parameters for cuprates.

These results lead to the conclusion that the initial relaxation process in Mott insulators coupled to phonons is governed by the phonon degree of freedom in 1D and by the spin degree of freedom in 2D. This may give a hint for the interpretation of ultrafast photo dynamics observed in 1D insulating cuprates [6] and organic materials [7–9] as well as 2D insulating cuprates [10].

I thank S. Sota, H. Matsueda, S. Maekawa, L. Vidmar, J. Bonča, and H. Lu for valuable discussions and collaboration. This work was supported by the Grant-in-Aid for Scientific Research (22340097) from MEXT, the Strategic Programs for Innovative Research (SPIRE), the Computational Materials Science Initiative (CMSI), the global COE program "Next Generation Physics, Spun from Universality and Emergence" from MEXT, the Yukawa International Program for Quark-Hadron Sciences at YITP, Kyoto University, and Slovnia-Japan collaboration project from ARRS and JSPS.

References

1. This issue of Euro. J. Phys.
2. See, for instance, S, Maekawa, T. Tohyama, S. E. Barnes, S. Ishihara, W. Koshibae, and G. Khaliullin, *Physics of Transition Metal Oxides* (Springer-Verlag, Berlin, 2004).
3. S. Sota and T. Tohyama, Phys. Rev. B **82**, 195130 (2010)
4. H. Matsueda, S. Sota, T. Tohyama, and S. Maekawa, J. Phys. Soc. Jpn. **79**, 013701 (2012)
5. L. Vidmar, J. Bonca, T.Tohyama, and S. Maekawa, Phys. Rev. Lett. **107**, 246404 (2011)
6. T. Ogasawara, M. Ashida, N. Motoyama, H. Eisaki, S. Uchida, Y. Tokura, H. Ghosh, A. Shukla, S. Mazumdar, and M. Kuwata-Gonokami, Phys. Rev. Lett. **85**, 2204 (2000)
7. S. Iwai, M. Ono, A. Maeda, H. Matsuzaki, H. Kishida, H. Okamoto, and Y. Tokura, Phys. Rev. Lett. **91**, 057401 (2003)
8. H. Okamoto, H. Matsuzaki, T. Wakabayashi, Y. Takahashi, and T. Hasagawa, Phys. Rev. Lett. **98**, 037401 (2007)
9. H. Uemura, H. Matsuzaki, Y. Takahashi, T. Hasegawa, and H. Okamoto, J. Phys. Soc. Jpn. **77**, 113714 (2008)
10. H. Okamoto, T. Miyagoe, K. Kobayashi, H. Uemura, H. Nishioka, H. Matsuzaki, A. Sawa, and Y. Tokura, Phys. Rev. B **83**, 125102 (2011)
11. M. Nagai and M. Kuwata-Gonokami, J. Phys. Soc. Jpn. **71**, 2276 (2011)
12. H. Kishida, H. Matsuzaki, H. Okamoto, T. Tanabe, M. Yamashita, Y. Taguchi, and Y. Tokura, Nature (London) **405**, 929 (2000)
13. A. Takahashi, H. Itoh, and M. Aihara, Phys. Rev. B **77**, 205105 (2008)
14. T. Oka and H. Aoki, Phys. Rev. B **78**, 241104 (2008)

15. K. A. Al-Hassanieh, F. A. Reboredo, A. E. Feiguin, I. González, and E. Dagotto, Phys. Rev. Lett. **100**, 166403 (2008)
16. O. Rösch and O. Gunnarsson, Phys. Rev. Lett. **92**, 146403 (2004)
17. O. Rösch and O. Gunnarsson, Phys. Rev. B **70**, 224518 (2004)
18. E. Jeckelmann, Phys. Rev. B **66**, 045114 (2002)
19. H. Suzuura, H. Yasuhara, A. Furusaki, N. Nagaosa, and Y. Tokura, Phys. Rev. Lett. **76**, 2579 (1996)
20. A. Weiße, G. Wellein, A. Alvermann, and H. Fehske, Rev. Mod. Phys. **78**, 275 (2006)
21. R. Neudert, M. Knupfer, M. S. Golden, J. Fink, W. Stephan, K. Penc, N. Motoyama, H. Eisaki, and S. Uchida, Phys. Rev. Lett. **81**, 657 (1998)
22. H. Matsueda, T. Tohyama, and S. Maekawa, Phys. Rev. B **70**, 033102 (2004)
23. H. Matsueda, T. Tohyama, and S. Maekawa, Phys. Rev. B **71**, 153106 (2005)
24. W. Stephan and K. Penc, Phys. Rev. B **54**, R17269 (1996)
25. Y.-J. Kim, J. P. Hill, H. Benthien, F. H. L. Essler, E. Jeckelmann, H. S. Choi, T. W. Noh, N. Motoyama, K. M. Kojima, S. Uchida, D. Casa, and T. Gog, Phys. Rev. Lett. **92**, 137402 (2004)
26. H. Benthien and E. Jeckelmann, Phys. Rev. B **75**, 205128 (2007)
27. A. S. Mishchenko and N. Nagaosa, Phys. Rev. Lett. **93**, 036402 (2004)
28. N. Motoyama, H. Eisaki, and S. Uchida, Phys. Rev. Lett. **76**, 3212 (1996)
29. J. Lorenzana and R. Eder, Phys. Rev. B **55**, R3358 (1997)
30. M. Ono, K. Miura, A. Maeda, H. Matsuzaki, H. Kishida, Y. Taguchi, Y. Tokura, M. Yamashita, and H. Okamoto, Phys. Rev. B **70**, 085101 (2004)
31. H. Matsueda, A. Ando, T. Tohyama, and S. Maekawa, Phy. Rev. B **77**, 193112 (2008)
32. J. Bonča, S. Maekawa, and T. Tohyama, Phys. Rev. B **76**, 035121 (2007)
33. J. Bonča, S. Maekawa, T. Tohyama, and P. Prelovšek, Phys. Rev. B **77**, 054519 (2008)
34. L. Vidmar, J. Bonča, S. Maekawa, and T. Tohyama, Phys. Rev. Lett. **103**, 186401 (2009)
35. T. J. Park and J. C. Light, J. Chem. Phys. **85**, 5870 (1986)
36. A. S. Mishchenko and N. Nagaosa, Phys. Rev. Lett. **93**, 036402 (2004)
37. A. S. Mishchenko, *et al*, Phys. Rev. Lett. **100**, (2008) 166401
38. G. De Filippis, *et al*, Phys. Rev. B **80**, 195104 (2009)
39. L. Vidmar, J. Bonča, and S. Maekawa, Phys. Rev. B **79**, 125120 (2009)